Charge avalanches and depinning in the Coulomb glass: The role of long-range interactions

Juan Carlos Andresen,[1,2] Yohanes Pramudya,[3] Helmut G. Katzgraber,[4,5,6] Creighton K. Thomas,[7] Gergely T. Zimanyi,[8] and V. Dobrosavljević[3]

[1]*Theoretische Physik, ETH Zurich, CH-8093 Zurich, Switzerland*
[2]*Department of Theoretical Physics, Royal Institute of Technology, Stockholm, Sweden*
[3]*Department of Physics and National High Magnetic Field Laboratory, Florida State University, Tallahassee, Florida 32306, USA*
[4]*Department of Physics and Astronomy, Texas A&M University, College Station, Texas 77843-4242, USA*
[5]*Santa Fe Institute, 1399 Hyde Park Road, Santa Fe, New Mexico 87501, USA*
[6]*Applied Mathematics Research Centre, Coventry University, Coventry, CV1 5FB, United Kingdom*
[7]*Department of Materials Science and Engineering, Northwestern University, Evanston, Illinois 60208-3108, USA*
[8]*Department of Physics, University of California, Davis, California 95616, USA*

(Received 11 September 2013; revised manuscript received 4 February 2016; published 24 March 2016; corrected 13 June 2016)

We explore the stability of far-from-equilibrium metastable states of a three-dimensional Coulomb glass at zero temperature by studying charge avalanches triggered by a slowly varying external electric field. Surprisingly, we identify a sharply defined dynamical ("depinning") phase transition from stationary to nonstationary charge displacement at a critical value of the external electric field. Using particle-conserving dynamics, scale-free system-spanning avalanches are observed only at the critical field. We show that the qualitative features of this depinning transition are completely different for an equivalent short-range model, highlighting the key importance of long-range interactions for nonequilibrium dynamics of Coulomb glasses.

DOI: 10.1103/PhysRevB.93.094429

I. INTRODUCTION

The long-range nature of the Coulomb interaction plays only a secondary role in metals, where it remains screened by mobile electrons down to atomic length scales. The situation is, however, far more interesting on the insulating side of disorder-driven metal-insulator transitions [1], where screening is suppressed due to charge localization. Here, the unscreened Coulomb interaction leads to the opening of the "Coulomb gap" in the electronic density of states, as first pointed out in pioneering works of Pollack [2], as well as Efros and Shklovskii (ES). The ES theory [3,4] predicts a universal form of the Coulomb gap, and explains how its existence modifies hopping transport [4] in disordered insulators, consistent with numerous experiments [5]. Early work also revealed that Coulomb interactions in disordered insulators generally contribute to the formation of an extensive number of metastable states, i.e., the formation of the Coulomb glass (CG) [6–8]. In subsequent work, various aspects of glassy behavior of the CG were explored theoretically [9–18] and experimentally [19–31].

More recent progress followed with the formulation of analytical theories of the CG [10–13,16,17], which adapted Parisi's replica methods [32–35] for spin glasses to disordered Coulomb systems. These theories find a Coulomb gap of the same universal form as predicted by the ES theory, but this behavior emerges only within the low-temperature glassy phase (displaying replica symmetry breaking). Within this mean-field picture, the universality of the Coulomb gap, as well as the saturation of the appropriate stability bound, can be directly traced back to the "marginal stability" of the entire glassy phase [10]. In physical terms, the marginal stability reflects the emergence of "replicons," soft (gapless) collective excitations involving simultaneous rearrangements of many electrons. If such soft excitations indeed characterize the Coulomb glass, they should also govern the physical response to various weak perturbations (e.g., the external electric fields), perhaps leading to large-scale avalanches. Precisely such behavior has already been established [36,37] for infinite-range spin-glass models, leading to scale-free avalanches characterizing an entire manifold of metastable states. Despite the successes of the mean-field approach, its applicability to finite space dimensions remains the subject of much controversy and debate [38–43]. Furthermore, a computational search for a finite-temperature glass transition in the CG in two and three space dimensions has remained inconclusive [14,15,18]. To shed additional light on the nature of excitations in the CG, and further test the mean-field ideas, it is therefore useful to examine the stability of the low-lying metastable states by external electric fields.

In this work, we investigate the out-of-equilibrium behavior of a three-dimensional Coulomb glass at zero temperature and study the hopping and total charge displacement avalanches triggered by increasing an externally-applied electric field. Previous work on avalanches in the CG in three space dimensions done by Palassini and Goethe [44], which trigger avalanches via dipole excitations or charge insertions, find scale-free behavior for long-range hopping dynamics, but when hopping is bounded by a finite fixed range they do not find any scale-free avalanches. Because physical electrons rearrange themselves by finite-range hopping it is of interest to search for a scale-free behavior in the CG for bounded hopping dynamics by other means.

Here we study the CG with particle-number-conserving short-range hopping, by "adiabatically" increasing an external electric field up to a depinning electric field $\mathcal{E}_{\rm dp}$ that separates the steady current state from just finite electron rearrangements as a reaction to the external field. We find that scale-free avalanches arise in the Coulomb glass when the electric

 ©2016 American Physical Society

field is close to $\mathcal{E}_{\rm dp}$. To emphasize the role played by the long-range Coulomb interactions we repeat our simulations for an equivalent short-range interacting model. In this case we still find a sharply defined depinning transition, but a completely different form for the critical behavior. Here we do not find any scale-free avalanches, in dramatic contrast to the behavior of the CG model.

The outline of this paper is as follows. Section II describes the model, followed by a description of the used numerical procedure in Sec. III A. Measured quantities are introduced in Sec. III B, followed by results presented in Sec. IV.

II. MODEL

The Coulomb glass Hamiltonian (in dimensionless units) is given by [3]

$$\mathcal{H} = \frac{1}{2}\sum_{i\neq j}(n_i - K)\frac{1}{|\mathbf{r}_i - \mathbf{r}_j|}(n_j - K) + \sum_i n_i\varphi_i, \quad (1)$$

where n_i is the electron number at site i, K is the filling factor, $\mathbf{r}_i$ is the coordinate of site i, and φ_i a randomly-distributed on-site energy. For a charge neutral system, i.e., $K = 1/2$, in a constant external electric field $\mathcal{E}$ in x direction, Eq. (1) can be rewritten in an Ising spin formulation by setting [6] $S_i = 2n_i - 1$ ($S_i \in \{\pm 1\}$ an Ising spin variable)

$$\mathcal{H} = \frac{1}{4}\sum_{i<j} J_{ij}S_iS_j + \sum_i S_i(\Phi_i + V_i), \quad (2)$$

where the electric potential is $V_i = -\mathcal{E}x_i$ and x_i is the x position of spin i. This form of the Hamiltonian with $\mathcal{E} = 0$ is of a random-field Ising model with long-range antiferromagnetic interactions given by

$$J_{ij} = \frac{1}{|\mathbf{r}_i - \mathbf{r}_j|}. \quad (3)$$

The site energy $\Phi_i = \varphi_i/2$ is sampled from a Gaussian distribution with zero mean and standard deviation $\sigma = 0.5$. To keep the dynamics of the two models identical it is necessary to constrain the Ising-like Hamiltonian in Eq. (2) to have a constant magnetization ($m = 0$ for $K = 1/2$) at all times. This is accomplished by using magnetization-conserving Kawasaki dynamics [45].

The corresponding short-range model (SR) is given by the same Hamiltonian in Eq. (2), but with long-range interactions replaced by nearest-neighbor interactions (on a cubic lattice) of the form

$$J_{ij} = \begin{cases} 1 & \text{if } i \text{ and } j \text{ are nearest neighbors,} \\ 0 & \text{otherwise.} \end{cases} \quad (4)$$

A. Determination of the initial configurations

In our simulations, we need to generate stable initial configurations of the system. In this context, "stable" refers to stable towards single nearest-neighbor electron hopping. We implement this procedure for both the CG and the SR model. In order to have an initial configuration with a Coulomb gap and track its dependence on the electric field, we compute pseudo-ground-state configurations using jaded extremal optimization (JEO) [46].

The single-particle density of states (DOS) of a classical Coulomb system is given by

$$\rho(E) = \left\langle \frac{1}{N}\sum_i \delta(E - E_i) \right\rangle, \quad (5)$$

where the local single-particle energy is given by

$$E_i = \frac{1}{2}\sum_j J_{ij}S_i + 2\Phi_i i = \sum_j \left(n_i - \frac{1}{2}\right)J_{ij} + \varphi_i, \quad (6)$$

and the average $\langle\cdots\rangle$ is performed both over thermal fluctuations and disorder instances. The ground state of the CG is well known to display a Coulomb gap [3] in the DOS at the Fermi energy, which gradually fills up when temperature is increased [6,7,9,18,47].

For the CG, we can empirically check how "far" or "close" a given configuration is from the ground state by examining the form of the DOS. Depending on the depth of the Coulomb gap, we can argue whether the configurations are close or far from their respective ground state. The SR ground states do not have a Coulomb gap [40], but have a "dip" at the Fermi energy that converges to a finite value in the thermodynamic limit. Again, we can empirically check if we have a good approximation of the ground state by studying at the DOS distribution. In Fig. 1(a), we show the DOS of the CG using the pseudoground states for all simulated linear system sizes L (the systems have $N = L^3$ spins). The occupation at $E = 0$ is very close to zero, showing that the configurations found using JEO are not far from the true ground state. In Fig. 1(b), we show the DOS of the CG at electric fields $0.5 < \mathcal{E} < 0.6$. The data suggest that we are further away from a ground-state configuration, however, a pronounced gap in the DOS is still visible. The configurations for the SR model found by the JEO algorithm are likewise not far from the ground state (not shown).

III. NUMERICAL DETAILS

A. Algorithm

For the description of the algorithm, we introduce a stability criterion, which for an electron ($S_i = 1$) or a vacancy ($S_i = -1$) at a given site is given by

$$(E_i + V_i)\cdot S_i < 0 \quad \rightarrow \quad \text{stable}, \quad (7)$$

$$(E_i + V_i)\cdot S_i > 0 \quad \rightarrow \quad \text{unstable}. \quad (8)$$

For each pseudoground state generated via JEO [see Fig. 1(a)], we proceed as follows. (1) Select the least stable electron with one nearest-neighbor hole in the opposite direction of the electric field. (2) Apply an electric field $\mathcal{E}$ just strong enough to destabilize the selected electron, such that it will hop to the neighboring hole. (3) Recompute all single-particle energies given by Eq. (6), and select the most unstable electron that minimizes the total energy by hopping to one of its neighboring holes. If there are no unstable electrons or an energy minimization is not possible, go to step 3. (4) Perform the electron-hole hopping that minimizes the energy; go to step III A.

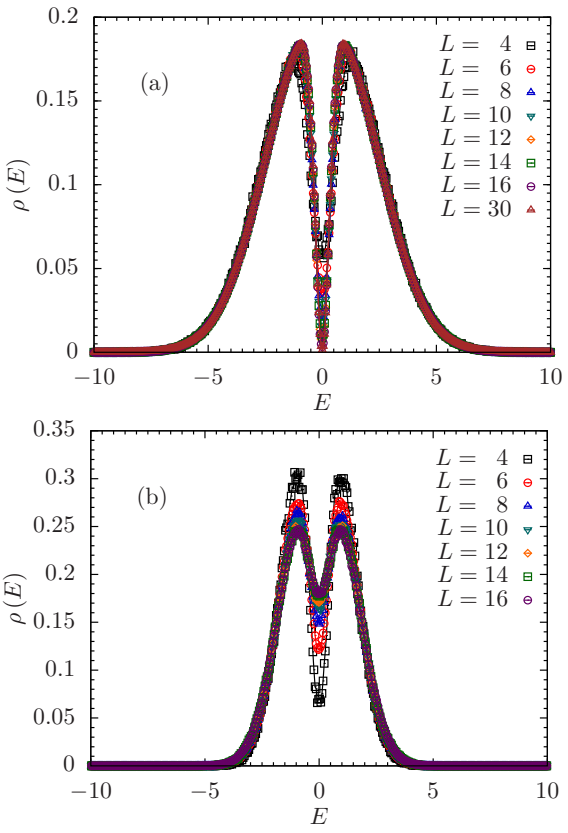

FIG. 1. Density of states for the three-dimensional CG of (a) the starting pseudo-ground-state configurations and (b) over a range of different electric potentials $0.5 < \mathcal{E} < 0.6$. Both distributions show a clear dip for $E = 0$, suggesting that the states computed using JEO are indeed close to the true ground state of the system. Data averaged over 2500–10 000 disorder instances, depending on the size size of the system (see Table I).

The careful reader will have noticed that the above procedure is in fact an infinite loop stuck between steps 3 and 4 when a certain electric field threshold $\mathcal{E} \geq \mathcal{E}_{\rm dp}$ is reached. This electric field threshold is the depinning field of the system, which separates two regions; below $\mathcal{E}_{\rm dp}$, there are only short charge displacement pulses due to the rearrangement of the electrons as a response to the external electric field, and above it there is a steady current. A sketch of the different scenarios is shown in Fig. 2. The infinite loop between 3 and step 4 is the steady current flowing through the system. Since we are interested in the number of times step 3 and step 4 are repeated at each $\mathcal{E}$ field (this, in turn, yields the avalanche size n) before we reach the depinning field, we artificially stop the process if the avalanche size surpasses a given number $n_{\rm steady} = 2N$, where N is the total number of sites of the system. Note that $n_{\rm steady}$ is much larger than the maximal avalanche size measured for $\mathcal{E} < \mathcal{E}_{\rm dp}$ for a given system size L.

To cope with the long-range Coulomb interactions between the electrons we use the Ewald summation method [48]. Furthermore, the applied electric field is periodic to avoid an electron pileup at the edge of the system. The simulation parameters are listed in Table I.

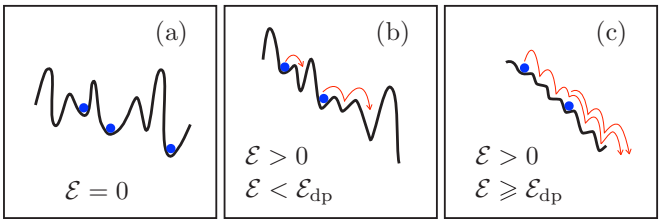

FIG. 2. Sketch of the site-dependent random potential landscape felt by the electrons (blue circles) at different electric field strengths: (a) $\mathcal{E} = 0$, (b) $0 < \mathcal{E} < \mathcal{E}_{\rm dp}$, and (c) $\mathcal{E}_{\rm dp} \leq \mathcal{E}$. (a) Stable configuration of electrons at $\mathcal{E} = 0$. (b) The electric field effectively tilts the potential. At electric fields $0 < \mathcal{E} < \mathcal{E}_{\rm dp}$ the electrons just rearrange as a reaction to the field. (c) The electric field $\mathcal{E} \geq \mathcal{E}_{\rm dp}$ further tilts the potential to a point where a steady current is induced.

B. Measured observables and statistical data analysis

At each increase of $\mathcal{E}$ we count the number of electrons n that hopped and the total charge displacement S in the direction of the applied electric field. Using these data, we compute their distributions $D(n)$ and $P(S)$, respectively (see, for example, Fig. 3). To determine the depinning field $\mathcal{E}_{\rm dp}$ we compute the cumulative distribution function $P_0(L,\mathcal{E})$ of the depinning distributions which gives the probability whether a randomly picked sample is in the pinned or depinned state for a given system size and at a given field. We perform a finite-size scaling assuming that the function P_0 has a universal form [50–52]

$$P_0 \sim \tilde{\Phi}[L^{1/\nu}(\mathcal{E}/\mathcal{E}_{\rm dp} - 1)] \tag{9}$$

[see Fig. 5(b) and Fig. 8(b) for the CG model and the SR model, respectively], which gives us an estimate of the depinning field. Note that the depinning field is defined as the typical electric field necessary to induce a continuous current for a given system size, i.e, for $\mathcal{E} < \mathcal{E}_{\rm dp}$, the system just rearranges its electron configuration by electron hopping, whereas for $\mathcal{E} > \mathcal{E}_{\rm dp}$, the field induces a steady current.

TABLE I. Parameters of the simulation: For the Coulomb glass (CG) and the short-range model (SR), we study systems of $N = L^3$ spins close to the ground state and compute the different distributions over $N_{\rm sa}$ disorder samples for different applied electric fields $\mathcal{E}$.

Model	L	$N_{\rm sa}$
CG	4	8000
CG	6	9000
CG	8	6500
CG	10	5000
CG	12	4000
CG	14	9000
CG	16	4000
CG	30	2500
SR	4	12 000
SR	8	14 400
SR	16	10 200
SR	24	9500
SR	32	7400
SR	48	2500
SR	64	700

In addition, we define the characteristic avalanche size n^* of the system by fitting the exponential tail of the avalanche distributions $D(n)$ to an exponential function $\sim \exp(-n/n^*)$. For each system size L, we thus obtain a characteristic avalanche size $n^*(L)$. To estimate the value of n^*_∞ in the thermodynamic limit, we do an extrapolation of $n^*_{L\to\infty}$ by using the following functional ansatz:

$$1/n^*_L = 1/n^*_\infty + a/L^\omega, \tag{10}$$

where ω, a, and n^*_∞ are fitting parameters.

Finally, we also monitor the DOS as a function of the applied electric field $\mathcal{E}$. For example, Fig. 1(b) shows the density of states at an electric field range of $0.5 < \mathcal{E} < 0.6$.

Different finite-size scaling Ansätze have been attempted [36] to scale the $D(n)$ and $P(S)$ data without yielding any satisfactory results. We therefore empirically resized the avalanche curves without making any a priori assumptions. Interestingly, the following scaling ansatz showed good results:

$$D = \frac{1}{L}\, d(n/L), \tag{11}$$

$$P = \frac{1}{L}\, p(S/L), \tag{12}$$

where $d(n/L)$ and $p(S/L)$ in Eqs. (11) and (12), respectively, are universal functions.

IV. RESULTS

Figure 3 shows electron hop, as well as total charge displacement avalanche distributions for the CG for different ranges of the electric field $\mathcal{E}$. The field $\mathcal{E}$ is increased in the different panels from top to bottom. Figures 3(a)–3(c) show how the avalanche sizes progressively become system spanning, i.e., when $\mathcal{E} \approx \mathcal{E}_{\rm dp}$ [as is the case in Fig. 3(c)] avalanche size distributions become power laws. As the field reaches $\mathcal{E}_{\rm dp}$ a hunch in the curves emerges separating a power-law region from an exponential cutoff, for the measured avalanches distribution $D(n)$. Figure 6 shows the dependence of the inverse of the characteristic avalanche size $1/n^*$ as a function of the electric field $\mathcal{E}_{\rm dp}$. We can extract from the figure that the depinning field $\mathcal{E}_{\rm dp}$ lies somewhere around $\mathcal{E} \approx 0.6$. A precise estimate of the depinning field can be obtained by analyzing the cumulative distribution function P_0 as shown in Fig. 5(b). For the CG model we obtain $\mathcal{E}_{\rm dp} = 0.609(7)$. In Fig. 7, we show an example of the estimation of n^* using Eq. (10) for a given field window $0.5 < \mathcal{E} < 0.6$. Similar qualitative results are obtained for the charge displacement distribution $P(S)$, as shown in Fig. 3(d). We attempt to scale the data for the distributions $D(n)$ and $P(S)$ in Fig. 4. The data scale well with no adjustable parameters (especially for the larger system sizes) according to Eqs. (11) and (12).

In addition, we study the total charge displacement distribution and electron hop distribution as a function of the applied field for the SR model, where the estimated depinning field is $\mathcal{E}_{\rm dp} = 0.781(9)$ as seen in Fig. 8. Electron avalanche distributions are shown in Fig. 9. For low fields, i.e., $\mathcal{E} < 0.5$, the characteristic avalanche size $n^*(L)$ can be estimated analogously as for the CG model, i.e., fitting the tail to an exponential function and using Eq. (10) to extrapolate to the thermodynamic limit. As for the CG model at low fields,

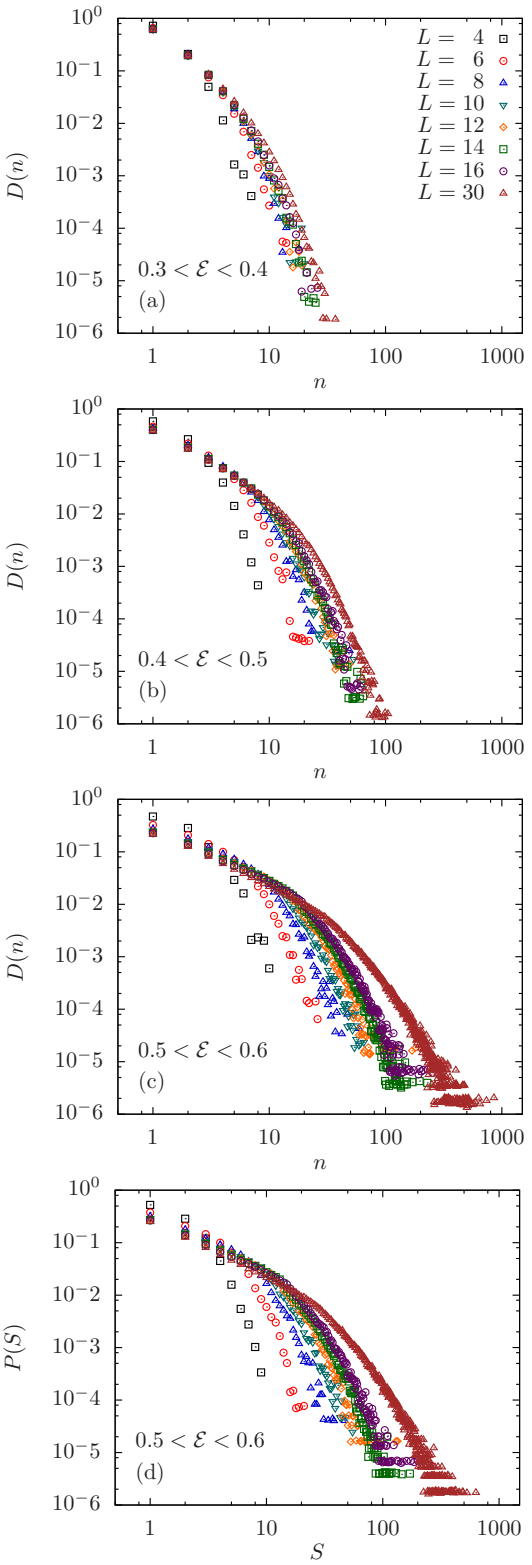

FIG. 3. (a), (b), and (c) show electron-hole avalanche distributions $D(n)$ of the CG at electric field ranges between $0.3 < \mathcal{E} < 0.6$. Scale-free avalanches emerge as $\mathcal{E}$ approaches $\mathcal{E}_{\rm dp} \approx 0.603(5)$. (a) $0.3 < \mathcal{E} < 0.4$, (b) $0.4 < \mathcal{E} < 0.5$, and (c) $0.5 < \mathcal{E} < 0.6$. Note that only close to the depinning electric field $\mathcal{E}_{\rm dp} \approx 0.603(5)$ scale-free avalanches, i.e., power-law distributions of avalanche sizes, emerge. (d) Distribution of charge displacement spikes (avalanches) $P(S)$ of the CG for $0.5 < \mathcal{E} < 0.6$.

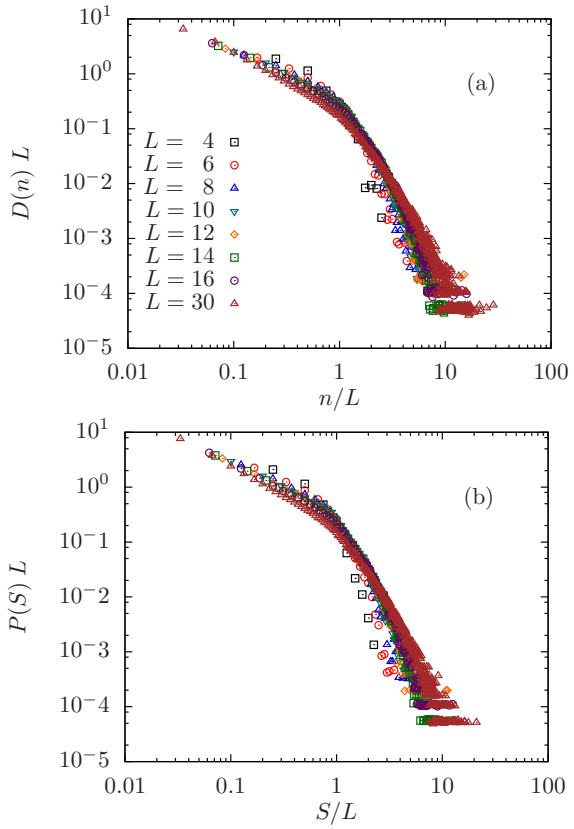

FIG. 4. Finite-size scaling data collapse of the electron avalanche distributions $D(n)$ (a) according to Eq. (11) with $0.5 < \mathcal{E} < 0.6$, i.e., close to $\mathcal{E}_{\rm dp}$. For the largest system sizes the data seem to collapse well. (b) shows a data collapse of the charge displacement distributions $P(S)$ according to Eq. (12) with $0.5 < \mathcal{E} < 0.6$. Again, the data scale well. Note that the symbols used are the same as in (a).

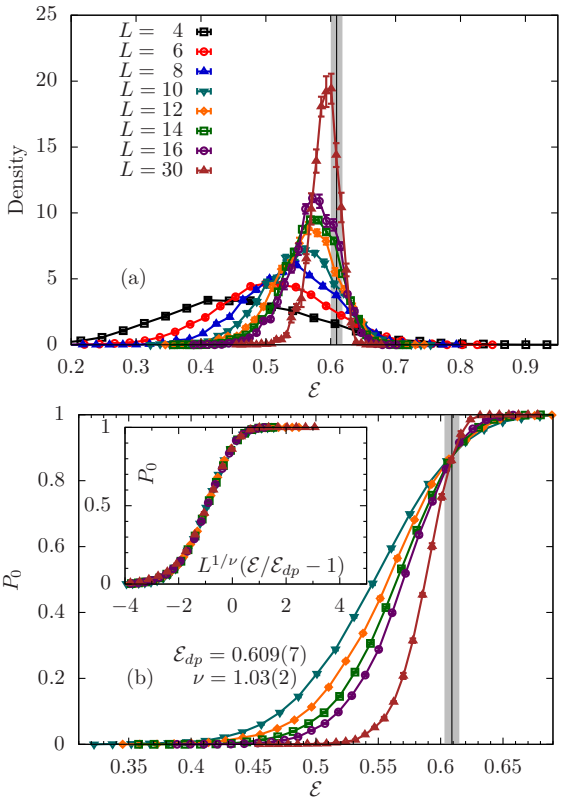

FIG. 5. (a) Depinning distributions for all system sizes studied of the CG model. The vertical line represents the estimated depinning field $\mathcal{E}_{\rm dp}$. (b) The cumulative distribution function of the depinning field for linear system sizes $L \geqslant 10$. The curves for different system sizes cross a the depinning field value. The inset is a data collapse assuming the universal function P_0 scales as Eq. (9).

no system-spanning avalanches were found, moreover no emergent avalanche size dependence is observed [Figs. 9(a) and 9(b)]. For fields closer to the depinning field, i.e., $\mathcal{E} \gtrsim 0.5$, the exponential fitting function [Eq. (10)] gives unsatisfactory fitting results, therefore we additionally fitted the distribution to a stretched exponential function

$$f(x) = a_L \ \exp[-(x/n_L^*)^{\beta_L}]. \tag{13}$$

The characteristic avalanche size n^* defined through the stretched exponential function is bounded in the thermodynamic limit for all fields, especially close to the depinning field: the inset of Fig. 9(d) shows the values of n^* for the field window $0.72 < \mathcal{E} < 0.77$. The stretched exponential exponent β has a strong field dependence as seen in Fig. 10. At low fields $\beta \approx 0.8$ and as the field increases it monotonically decreases to $\beta \approx 0.2$ [53].

We observe that the CG model and the SR model have a well defined depinning field transition, but that they differ in the way they behave close to $\mathcal{E}_{\rm dp}$. The CG model total charge displacement and electron hop avalanche distributions close to the depinning field have a power-law shape (with power-law exponent $\tau \approx -1$) with a system-size dependent exponential cutoff. This finite-size effect vanishes in the thermodynamic limit, revealing its scale-free behavior at $\mathcal{E}_{\rm dp}$. In clear contrast the SR model total charge displacement and electron hop avalanche distributions show no signs of scale-free avalanche behavior (power-law shape) close to $\mathcal{E}_{\rm dp}$ and are best described by a stretched exponential function, which is defined by the exponent β and the parameter n^*. The exponent β shows a strong field dependence; it decreases monotonically as the field is increased, while n^* does not show any systematic

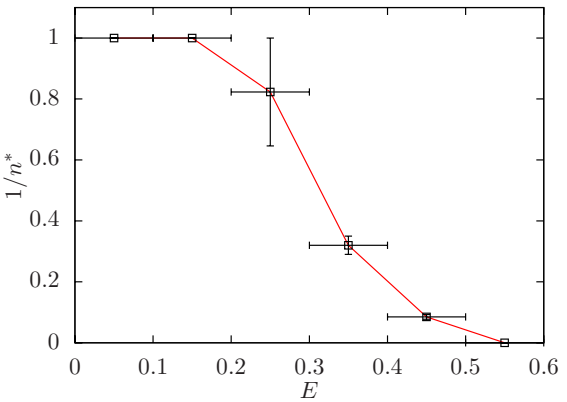

FIG. 6. Characteristic avalanche size n^*, computed using Eq. (10), as a function of the applied field $\mathcal{E}$ for the CG model. As the field increases, the inverse of the characteristic avalanche size $1/n^*$ decreases until at the depinning field $\mathcal{E}_{\rm dp}$ it becomes zero, i.e., $n^*(\mathcal{E}_{\rm dp}) \to \infty$ (the line is a guide to the eye).

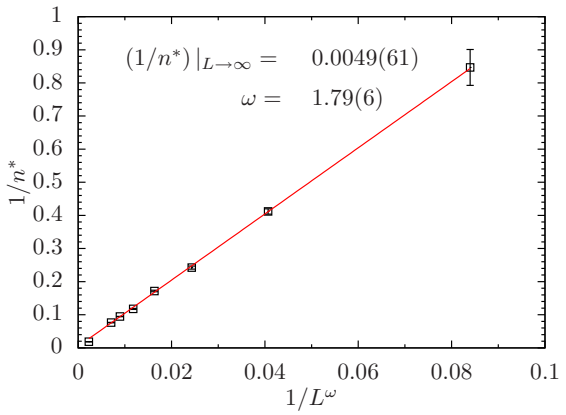

FIG. 7. Thermodynamic limit extrapolation of the characteristic avalanche size n^* for the CG model in an electric field $0.5 < \mathcal{E} < 0.6$ close the depinning field $\mathcal{E}_{dp} = 0.603(5)$. We fit the data to Eq. (10) with $1/n^*_\infty$, a, and ω parameters. An optimal fit gives $1/n^*_{CG} = 0.0049(61)$ [$\omega = 1.79(6)$] with a quality-of-fit probability [49] $Q = 0.994$. Note that fixing $1/n^*_\infty = 0$ gives $Q = 0.998$. This means that $n^*_\infty = \infty$, i.e., the presence of scale-free avalanches in this electric field regime.

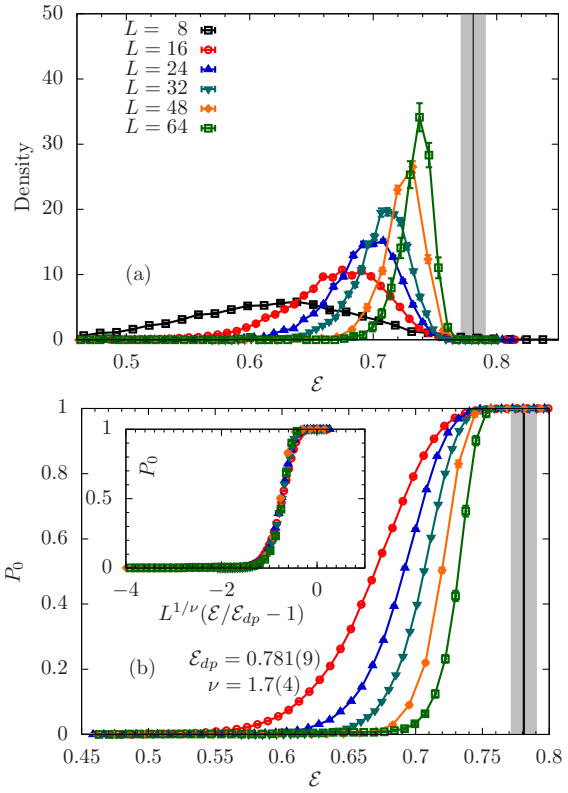

FIG. 8. (a) Depinning distributions for all system sizes studied of the SR model. The vertical line represents the estimated depinning field $\mathcal{E}_{dp}$. (b) The cumulative distribution function of the depinning field for linear system sizes $L \geqslant 16$. The curves for different system sizes cross a the depinning field value. Here the crossing seems to happen in a region where it is not possible to distinguish it. Nevertheless, as seen in the inset, assuming the universal function P_0 scales as shown in Eq. (9) the data collapse is satisfactory.

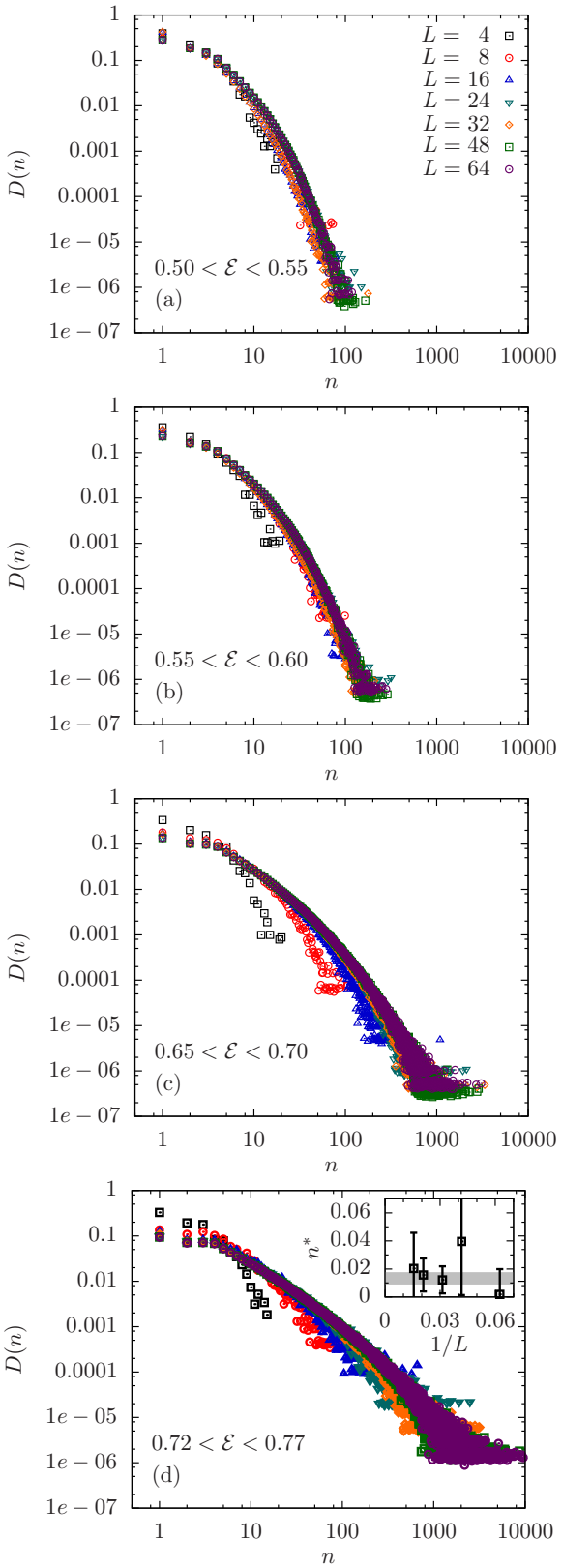

FIG. 9. Spin avalanches $D(n)$ of the SR model at different electric field ranges: (a) $0.50 < \mathcal{E} < 0.55$, (b) $0.55 < \mathcal{E} < 0.60$, (c) $0.65 < \mathcal{E} < 0.70$, and (d) $0.72 < \mathcal{E} < 0.77$. Even for $\mathcal{E} \approx \mathcal{E}^{SR}_{dp}$ (d), there is no sign of scale-free avalanches. The inset in (d) shows the n^* estimates for system sizes $L \geq 16$ and the gray horizontal line is their mean value.

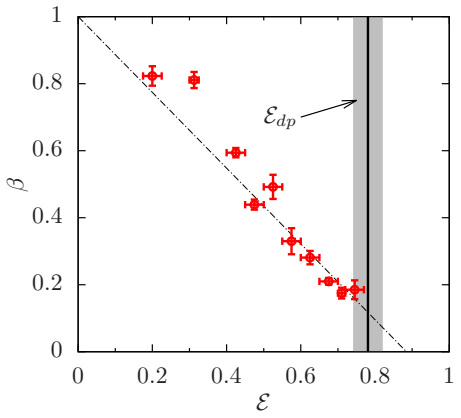

FIG. 10. Stretched exponential exponent β of the SR model as a function of the applied field $\mathcal{E}$. The exponent β decreases monotonically with the field. The vertical line shows the estimated depinning field $\mathcal{E}_{\rm dp}$ and the dashed line is a guide to the eye.

system-size dependence at any field, not even close to the depinning field. The different avalanche distributions in the SR and CG models hint towards a different mechanism behind the depinning transition.

V. CONCLUSIONS

Our large-scale computational study of the Coulomb glass has demonstrated that, under external electric fields and nearest-neighbor particle-conserving hopping dynamics, scale-free avalanches only occur in the vicinity of a characteristic depinning field $\mathcal{E}_{\rm dp}$. For small external electric fields, no large avalanches are present, in agreement with the results of Palassini and Goethe [44]. For a short-range variation of the Coulomb glass model, we do not find any sign of scale-free avalanches, not even close to the depinning electric field. Furthermore, we find that the initial Coulomb gap vanishes as the field is ramped up, suggesting that it is not a generic feature on the hysteresis loop formed in an external electric field. We empirically find a simple scaling ansatz to collapse the avalanche and charge displacement distributions, reinforcing the notion that the scale-free behavior of the CG emerges close to the depinning electric field.

The scale-free behavior found in the CG is not a self-organized critical (SOC) state, because an external parameter has to be tuned [37,54–56], namely, the electric field $\mathcal{E}$. Nevertheless, it is interesting to note the difference between the CG and the SR model: in the former the combination of the diverging number of neighbors and disorder results in power-law distributions, which is not the case in the latter. This behavior is very similar to that found for the three-dimensional random-field Ising model [57–61], where scale-free avalanches have been observed at a critical field strength h_c. These unexpected results for the Coulomb glass show that a diverging number of neighbors is necessary but *not* sufficient in a model Hamiltonian to show SOC behavior, and that the dynamics of a model might play an important role for showing SOC (i.e., the order-parameter conserving Kawasaki dynamics used here vs single-spin flip dynamics used for the random-field Ising model).

Our results bring into question the validity of the mean-field picture of the Coulomb glass [10–13,16,17], predicting extreme fragility of the ground state to external perturbations. However, the generic absence of SOC for avalanches driven by a uniform electric field may be related to the fact that such large avalanches *locally* violate charge neutrality. Other dynamical perturbations may couple differently to the elementary excitations and may perhaps serve as a more sensitive probe to the proposed SOC nature of the CG ground state. This could be achieved by applying external fields that do not directly couple to the *uniform* charge density, such as varying the amplitude of the disorder potential. Such or similar studies represent an opportunity to further elucidate the long-standing mystery of the Coulomb glass, however, exploring this exciting research direction remains a challenge for future work.

ACKNOWLEDGMENTS

We would like to thank R. S. Andrist for many discussions, as well as Mauricio Andresen for providing the necessary motivation to complete this project. V.D. and Y.P. were supported by the NSF Grants No. DMR-1005751 and No. DMR-1410132. G.T.Z. was supported by the NSF (Grant No. DMR-1035468). H.G.K. acknowledges support from the NSF (Grant No. DMR-1151387) and would like to thank ETH Zurich for CPU time on the Brutus cluster, as well as Aspall (Suffolk) for inspiration. Part of H.G.K.'s research is based upon work supported in part by the Office of the Director of National Intelligence (ODNI), Intelligence Advanced Research Projects Activity (IARPA), via MIT Lincoln Laboratory Air Force Contract No. FA8721-05-C-0002. The views and conclusions contained herein are those of the authors and should not be interpreted as necessarily representing the official policies or endorsements, either expressed or implied, of ODNI, IARPA, or the U.S. Government. The U.S. Government is authorized to reproduce and distribute reprints for Governmental purpose notwithstanding any copyright annotation thereon.

[1] V. Dobrosavljević, N. Trivedi, and J. M. Valles, *Conductor-Insulator Quantum Phase Transitions* (Oxford University Press, Oxford, England, 2012).
[2] M. Pollak, Disc. Faraday Soc. **50**, 13 (1970).
[3] A. L. Efros and B. I. Shklovskii, Coulomb gap and low temperature conductivity of disordered systems, J. Phys. C **8**, L49 (1975).
[4] B. I. Shklovskii and A. L. Efros, *Electronic Properties of Doped Semiconductors*, Springer Series in Solid-State Sciences, Vol. 45 (Springer Verlag, New York, 1988).
[5] P. A. Lee and T. V. Ramakrishnan, Disordered electronic systems, Rev. Mod. Phys. **57**, 287 (1985).
[6] J. H. Davies, P. A. Lee, and T. M. Rice, Electron Glass, Phys. Rev. Lett. **49**, 758 (1982).

[7] J. H. Davies, P. A. Lee, and T. M. Rice, Properties of the electron glass, Phys. Rev. B **29**, 4260 (1984).

[8] W. Xue and P. A. Lee, Monte Carlo simulations of the electron glass, Phys. Rev. B **38**, 9093 (1988).

[9] E. R. Grannan and C. C. Yu, Critical Behavior of the Coulomb Glass, Phys. Rev. Lett. **71**, 3335 (1993).

[10] A. A. Pastor and V. Dobrosavljević, Melting of the Electron Glass, Phys. Rev. Lett. **83**, 4642 (1999).

[11] A. A. Pastor, V. Dobrosavljević, and M. L. Horbach, Mean-field glassy phase of the random-field Ising model, Phys. Rev. B **66**, 014413 (2002).

[12] V. Dobrosavljević, D. Tanasković, and A. A. Pastor, Glassy Behavior of Electrons Near Metal-Insulator Transitions, Phys. Rev. Lett. **90**, 016402 (2003).

[13] M. Müller and L. B. Ioffe, Glass Transition and the Coulomb Gap in Electron Glasses, Phys. Rev. Lett. **93**, 256403 (2004).

[14] D. Grempel, Off-equilibrium dynamics of the two-dimensional Coulomb Glass, Europhys. Lett. **66**, 854 (2004).

[15] A. B. Kolton, D. R. Grempel, and D. Dominguez, Heterogeneous dynamics of the three-dimensional Coulomb Glass out of equilibrium, Phys. Rev. B **71**, 024206 (2005).

[16] S. Pankov and V. Dobrosavljević, Nonlinear Screening Theory of the Coulomb Glass, Phys. Rev. Lett. **94**, 046402 (2005).

[17] M. Müller and S. Pankov, Mean-field theory for the three-dimensional Coulomb glass, Phys. Rev. B **75**, 144201 (2007).

[18] B. Surer, H. G. Katzgraber, G. T. Zimanyi, B. A. Allgood, and G. Blatter, Density of States and Critical Behavior of the Coulomb Glass, Phys. Rev. Lett. **102**, 067205 (2009).

[19] M. Ben-Chorin, Z. Ovadyahu, and M. Pollak, Nonequilibrium transport and slow relaxation in hopping conductivity, Phys. Rev. B **48**, 15025 (1993).

[20] Z. Ovadyahu and M. Pollak, Disorder and Magnetic Field Dependence of Slow Electronic Relaxation, Phys. Rev. Lett. **79**, 459 (1997).

[21] A. Vaknin, Z. Ovadyahu, and M. Pollak, Aging Effects in an Anderson Insulator, Phys. Rev. Lett. **84**, 3402 (2000).

[22] S. Bogdanovich and D. Popovic, Onset of Glassy Dynamics in a Two-Dimensional Electron System in Silicon, Phys. Rev. Lett. **88**, 236401 (2002).

[23] A. Vaknin, Z. Ovadyahu, and M. Pollak, Nonequilibrium field effect and memory in the electron glass, Phys. Rev. B **65**, 134208 (2002).

[24] V. Orlyanchik and Z. Ovadyahu, Stress Aging in the Electron Glass, Phys. Rev. Lett. **92**, 066801 (2004).

[25] J. Jaroszyński, D. Popović, and T. M. Klapwijk, Magnetic-Field Dependence of the Anomalous Noise Behavior in a Two-Dimensional Electron System in Silicon, Phys. Rev. Lett. **92**, 226403 (2004).

[26] Z. Ovadyahu, Quench-cooling procedure compared with the gate protocol for aging experiments in electron glasses, Phys. Rev. B **73**, 214204 (2006).

[27] J. Jaroszyński and D. Popović, Nonexponential Relaxations in a Two-Dimensional Electron System in Silicon, Phys. Rev. Lett. **96**, 037403 (2006).

[28] J. Jaroszyński and D. Popović, Nonequilibrium Relaxations and Aging Effects in a Two-Dimensional Coulomb Glass, Phys. Rev. Lett. **99**, 046405 (2007).

[29] I. Raičević, J. Jaroszyński, D. Popović, C. Panagopoulos, and T. Sasagawa, Evidence for Charge Glasslike Behavior in Lightly Doped $La_{2-x}Sr_xCuO_4$ at Low Temperatures, Phys. Rev. Lett. **101**, 177004 (2008).

[30] I. Raičević, D. Popović, C. Panagopoulos, and T. Sasagawa, Non-Gaussian noise in the in-plane transport of lightly doped $La_{2-x}Sr_xCuO_4$: Evidence for a collective state of charge clusters, Phys. Rev. B **83**, 195133 (2011).

[31] P. V. Lin, X. Shi, J. Jaroszynski, and D. Popović, Conductance noise in an out-of-equilibrium two-dimensional electron system, Phys. Rev. B **86**, 155135 (2012).

[32] G. Parisi, Order Parameter for Spin-Glasses, Phys. Rev. Lett. **50**, 1946 (1983).

[33] R. Rammal, G. Toulouse, and M. A. Virasoro, Ultrametricity for physicists, Rev. Mod. Phys. **58**, 765 (1986).

[34] M. Mézard, G. Parisi, and M. A. Virasoro, *Spin Glass Theory and Beyond* (World Scientific, Singapore, 1987).

[35] *Spin Glasses and Random Fields*, edited by A. P. Young (World Scientific, Singapore, 1998).

[36] F. Pázmándi, G. Zaránd, and G. T. Zimányi, Self-Organized Criticality in the Hysteresis of the Sherrington-Kirkpatrick Model, Phys. Rev. Lett. **83**, 1034 (1999).

[37] J. C. Andresen, Z. Zhu, R. S. Andrist, H. G. Katzgraber, V. Dobrosavljević, and G. T. Zimanyi, Self-Organized Criticality in Glassy Spin Systems Requires a Diverging Number of Neighbors, Phys. Rev. Lett. **111**, 097203 (2013).

[38] A. P. Young and H. G. Katzgraber, Absence of an Almeida-Thouless line in Three-Dimensional Spin Glasses, Phys. Rev. Lett. **93**, 207203 (2004).

[39] H. G. Katzgraber and A. P. Young, Probing the Almeida-Thouless line away from the mean-field model, Phys. Rev. B **72**, 184416 (2005).

[40] S. Boettcher, H. G. Katzgraber, and D. Sherrington, Local field distributions in spin glasses, J. Phys. A **41**, 324007 (2008).

[41] T. Jörg, H. G. Katzgraber, and F. Krzakala, Behavior of Ising Spin Glasses in a Magnetic Field, Phys. Rev. Lett. **100**, 197202 (2008).

[42] H. G. Katzgraber, D. Larson, and A. P. Young, Study of the de Almeida-Thouless Line Using Power-Law Diluted One-Dimensional Ising Spin Glasses, Phys. Rev. Lett. **102**, 177205 (2009).

[43] D. Larson, H. G. Katzgraber, M. A. Moore, and A. P. Young, Spin glasses in a field: Three and four dimensions as seen from one space dimension, Phys. Rev. B **87**, 024414 (2013).

[44] M. Palassini and M. Goethe, Elementary excitations and avalanches in the Coulomb glass, J. Phys.: Conf. Ser. **376**, 012009 (2012).

[45] M. E. J. Newman and G. T. Barkema, *Monte Carlo Methods in Statistical Physics* (Oxford University Press Inc., New York, USA, 1999).

[46] A. A. Middleton, Improved extremal optimization for the ising spin glass, Phys. Rev. E **69**, 055701(R) (2004).

[47] M. Sarvestani, M. Schreiber, and T. Vojta, Coulomb Gap at Finite Temperatures, Phys. Rev. B **52**, R3820 (1995).

[48] Z. Wang and C. Holm, Estimate of the cutoff errors in the Ewald summation for dipolar systems, J. Chem. Phys. **115**, 6351 (2001).

[49] W. H. Press, S. A. Teukolsky, W. T. Vetterling, and B. P. Flannery, *Numerical Recipes in C* (Cambridge University Press, Cambridge, England, 1995).

[50] M. Dong, M. C. Marchetti, A. A. Middleton, and V. Vinokur, Elastic String in a Random Potential, Phys. Rev. Lett. **70**, 662 (1993).

[51] M. E. J. Newman and R. M. Ziff, Efficient Monte Carlo Algorithm and High-Precision Results for Percolation, Phys. Rev. Lett. **85**, 4104 (2000).

[52] B. Xi, M. B. Luo, V. M. Vinokur, and X. Hu, arXiv:cond-mat/1501.04436.

[53] We also applied a stretched exponential fitting function to the CG model avalanche distributions. The stretched exponent β for the CG model are in good agreement with an exponential function for fields $\mathcal{E} \lesssim 0.5$. Close to $\mathcal{E}_{\rm dp}$ the exponent β is $0.5 \lesssim \beta \lesssim 0.8$. Nevertheless, a pure exponential function still gives satisfactory fitting quality values.

[54] P. Bak, C. Tang, and K. Wiesenfeld, Self-Organized Criticality: An Explanation of $1/f$ Noise, Phys. Rev. Lett. **59**, 381 (1987).

[55] B. Drossel and F. Schwabl, Self-Organized Critical Forest-Fire Model, Phys. Rev. Lett. **69**, 1629 (1992).

[56] K. Schenk, B. Drossel, and F. Schwabl, Self-Organized Criticality in Forest-Fire Models, in *Computational Statistical Physics*, edited by K. H. Hoffmann and M. Schreiber (Springer-Verlag, Berlin, 2002), p. 127.

[57] J. P. Sethna, K. Dahmen, S. Kartha, J. A. Krumhansl, B. W. Roberts, and J. D. Shore, Hysteresis and Hierarchies: Dynamics of Disorder-Driven First-Order Phase Transformations, Phys. Rev. Lett. **70**, 3347 (1993).

[58] O. Perkovic, K. A. Dahmen, and J. P. Sethna, Avalanches, Barkhausen Noise, and Plain Old Criticality, Phys. Rev. Lett. **75**, 4528 (1995).

[59] O. Perkovic, K. A. Dahmen, and J. P. Sethna, Disorder-induced critical phenomena in hysteresis: Numerical scaling in three and higher dimensions, Phys. Rev. B **59**, 6106 (1999).

[60] M. C. Kuntz, O. Perkovic, K. A. Dahmen, B. W. Roberts, and J. P. Sethna, Hysteresis, Avalanches, and Noise: Numerical Methods, arXiv:cond-mat/9809122v2.

[61] J. P. Sethna, K. A. Dahmen, and O. Perkovic, Random-Field Ising Models of Hysteresis, arXiv:cond-mat/0406320v3.